TITLE:

Development of dynamic deployment simulation of thin composite layer for shape morphing structure

AUTHOR(S):

Nishikawa, M.; Nagata, K.; Naito, Y.; Hojo, M.; Matsuda, N.

DEVELOPMENT OF DYNAMIC DEPLOYMENT SIMULATION OF THIN COMPOSITE LAYER FOR SHAPE MORPHING STRUCTURE

M. Nishikawa[1], K. Nagata[1*], Y. Naito[1*], M. Hojo[1] and N. Matsuda[1]

[1]C3 KyotoDaigaku-Katsura, Nishikyo-ku, Kyoto, Kyoto, Japan, 615-8540,
Department of Mechanical Engineering and Science, Kyoto University,
nishikawa@me.kyoto-u.ac.jp
*Affiliation at the time when involved with the present work

Keywords: Shape Morphing Structure, Composite Materials, Finite Element Analysis, Dynamic Deployment Simulation

ABSTRACT

The present study attempted to develop a numerical method to deal with deployment dynamics of a thin composite layer for shape morphing structures, including space deployable structure based on shape memory polymer composites (SMPCs). We utilized a three-layer model based on finite element analysis using shell elements in order to model a thin composite layer. The three-layer model could deal with the difference between tension and bending properties of the thin composite layer. Employing this approach, we also attempted to model our deployment experiment. We observed and simulated the deployment dynamics when one end of the hemispherically curved composite layer was released. When the appropriate bending modulus was used for modeling the composites, the simulated dynamics was almost similar to the experimental results. Therefore, we concluded that the proposed simulation can reproduce the deployment dynamics of a thin composite layer well.

1 INTRODUCTION

For future aerospace applications, shape morphing composite structures have been researched for decades [1-3]. Especially, shape memory polymer composites (SMPCs) [4-7] have been investigated as one of the promising materials which enable shape morphing only through heating sources. The shape fixity and shape recovery properties of these SMPCs as temperature-dependent viscoelastic properties allows a large shape change, which is required for the applications to space deployable structures [8], for example. Recently, we investigated a thermally-activated deployment system using shape memory textile composites [9], and we demonstrated that the deployment ratio could be controlled by the heating condition applied to the composite. However, our previous discussion was limited to the deployment under quasi-static conditions. In actual applications, the deployment will progress by simultaneously applying heat to multiple hinged parts made of SMPCs, and the deployment sequence is an issue to be discussed. If we can deal with these issues, the SMPCs will become one of the best candidate materials for shape morphing structures, since they allow the simultaneous deployment and also enable us to control the deployment sequence by heating conditions. As for the folding feature, the layer thickness of the material used for our previous study was made to be thin as about 0.25 mm, and thus the structure would be very compact in the folded state, because in principle, the allowable minimum curvature radius would be 12.5 mm, if the elongation strain of the material is assumed as 1.0 %. Therefore, the SMPCs will offer design flexibility for shape morphing structures.

Since the deployable structure becomes flexible during the deployment process, the combination of multiple deployable parts cause the interaction of the deformation of these parts. The interaction of the deformation during deployment may lead to the possibility of the occurrence of unstable deployment. There was a report in Ref. [10] that a small energy unbalance caused unstable deployment of the thin membrane used for IKAROS (solar sail membrane), though this example was not an application of composite materials. It is important to ensure the stability of deployment in order to enhance the reliability in the successful deployment of space deployable structures. As another example, Neto et al. [11] revealed that when synthetic aperture radar (SAR) antenna made of composite materials was

unfolded using actuators at revolute joints, the deployment dynamics as measured by actuator angles and the angular velocity of the panels was different between rigid and flexible panel structures, and that the layup of composite materials also affected the deployment dynamics. More importantly, their comparison among rigid, isotropic flexible and composite material models demonstrated the necessity of using different actuation laws of the actuator, because the undesirable contact of truss and panels in the structure occurred in the case of the deformable panel and the torsional deformation had a significant influence on the deployment of the panel made of composite materials. Keli and Banik [12] conducted the dynamic deployment tests of a CFRP (Carbon Fiber Reinforced Plastics) thin shell, which modeled a rollable composite shell reflector, and observed the stowage to a cylindrical shape and the deployment to the original shape of the shell using a high-speed camera. They compared three different prototype shells of different laminate configurations, and the deployment dynamics (gull-wing motion, snap-through instability and tip motion) from a roll-stowed configuration to an unfolded configuration was significantly different among these different prototype shells. They also pointed out the existence of creep effects during the stowage. These previous researches imply that the deployment dynamics are closely related to the material properties; for example, the fiber orientation of composite materials. Thus the deployment dynamics should be discussed with consideration of the material properties of a thin composite layer for shape morphing structures.

In this context, we attempted to develop a numerical method to deal with deployment dynamics of a thin composite layer. Thus we proposed a dynamic deployment simulation of a thin layer made of CFRP plain-woven textile composites, employing a shell-element based approach. The characteristics of the model for a thin composite layer was a consideration of both tensile and bending properties using a three-layer model. Using the dynamic deployment simulation, we attempted to reproduce the dynamic deployment tests from a rolled configuration to an unfolded configuration and demonstrate the effectiveness of the proposed deployment simulation.

2   SIMULATION PROCEDURE

This section briefly describes the numerical procedure for our dynamic deployment simulation. Our dynamic simulation employed dynamic explicit finite element analysis with shell elements. The degenerated isoparameteric shell elements based on Reissner-Mindlin assumption in an embedded coordinate system and the updated Lagrangian formulation were used in order to deal with large rotation and large strains. The detailed formulation was referred to Ref. [13]. When we employed the embedded coordinate system, numerical stability was achieved. Otherwise, the simulation often caused a mismatch between the change of director vectors to define material principal axes and the deformation of the shell elements, so that the constitutive tensors transferred from the material axes to the element local axes had a severe error. In the update of the director vectors due to a large rotation was also considered using the finite rotation tensor.

Our previous study in Ref. [9] for the quasi-static deployment simulation revealed that for thin textile composites, tension and bending properties are significantly different and the bending flexibility should be appropriately modeled. For this purpose, three-layer model was useful to consider the difference between tension and bending properties. The three-layer model has three layers in thickness direction with different material properties. For the symmetry in thickness direction, the upper and bottom layers have the same material properties. The three-layer model was extended for the analysis with shell elements in the present study. In the shell element, we obtained the material properties of the three-layer model, relating to the tensile and bending moduli (E_t, E_b) of the composites, using Eq. (1).

$$E_t = \frac{1}{2}\sum_{i=1}^{n} w(i)E_*(i) , \quad E_b = \frac{3}{2}\sum_{i=1}^{n} w(i)\big(r_3(i)\big)^2 E_*(i) \tag{1}$$

where E_* is the modulus of the corresponding layer, n is the number of integration points in thickness direction (3 or 4), w is the weight of the integral, r_3 is the local coordinate in isoparametric elements.

Using the dynamic deployment simulation, we also attempted to model our deployment experiment from a rolled state to an unfolded state, as later described in detail in section 3 (Fig. 1). The model size was 125.6 mm (length) $\times$ 10.0 mm (width) $\times$ 0.22 mm(thickness). The density was set to 1.5 g/cm^3 as
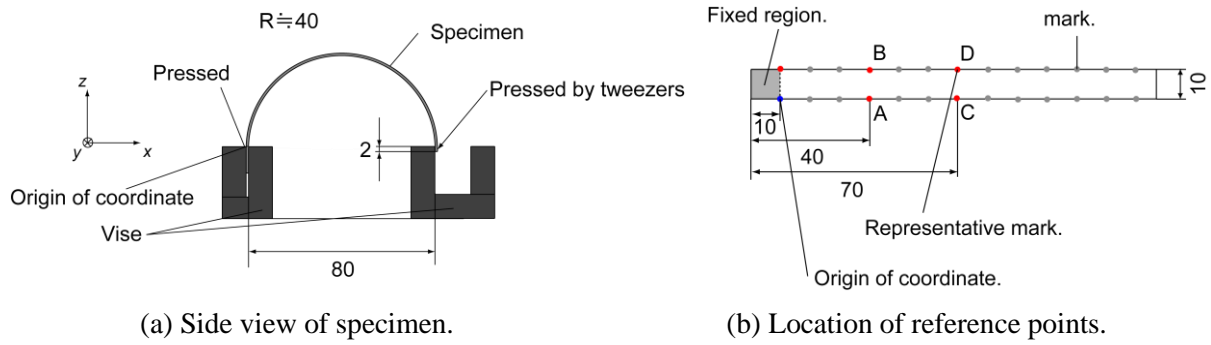
(a) Side view of specimen.   (b) Location of reference points.

Figure 1: Schematic of the dynamic deployment experiment (Unit: mm).

the averaged value of the used specimens. To eliminate the effect of membrane locking, 9-node elements with reduced integration (number of integration points = 12) was used. The number of elements was 10 in the model (in the length direction). The used material properties of the thin composite layer were those of CFRP in the experiment. Since the bending modulus of the specimen was unknown, the parameter study was conducted as it was varied as 12, 16, and 20 GPa. The tensile modulus was set as 32.8 GPa determined in Ref. [9], though the tensile modulus did not affect the results. The procedure of the dynamic deployment simulation consisted of two steps as follows.

(i) Deformation to constant curvature

The displacement/rotation boundary conditions were applied to all nodes so that the curvature $\kappa(t)$ linearly varied from 0 to 0.025 /mm within time between 0 s and 1 s. Thus, the boundary conditions were defined using the following equations as a function of time t ($0 < t < 1$s).

$$u_x = (1 - \cos l\kappa(t))/\kappa(t), \ u_y = 0, \ u_z = l(\sin(l\kappa(t))/\kappa(t) - 1) \tag{2}$$

$$\theta_\alpha = 0, \ \theta_\beta = l\kappa(t)$$

where l denotes the distance of each node from the fixed end at $t = 0$.

(ii) Release of the constraint and unfolding

The boundary conditions were fixed to zero for 3 nodes on one edge of the specimen. The boundary conditions applied to the remaining nodes were released.

3   DYNAMIC DEPLOYMENT TESTS

This section describes the procedure of dynamic deployment tests. We observed the deployment dynamics when one end of the hemispherically curved composite layer was released, and we attempted to reproduce the experimental results using the proposed deployment simulation.

The CFRP composite layer used in the experiment was made of CF/PU(polyurethane). Polyurethane used as the matrix was shape memory polymer (Diary MM5520, SMP technologies Inc.). The reinforcing material was CF plain-woven fabric (high-strength, intermediate-modulus CF, 3K, elastic modulus of CF: 230 GPa). The thin composite layer of CFRP was compression-molded; before the processing, a single layer of CF woven fabric was placed between two PU films. The specimen was cut to a rectangular shape of 137 mm (length) × 10 mm (width). The thickness was measured as 0.22 ± 0.01 mm. The photograph of a specimen used in the experiment was shown in Fig. 2.

The deployment dynamics was investigated by obtaining three-dimensional displacement of the specimen using a motion capture system with high-speed cameras. The reference points used for the motion capture were painted with a white marker, and the number of the reference points was 52 with 10 mm interval. In order to detect the reference points easily during the image processing, the additional lines were drawn so as to connect the reference points in the width direction of the specimen. The representative reference points A to D were shown in Fig. 1(b).

Fig. 1(a) depicts the experimental setup. Two vises for fixing the specimen were placed with 80 mm interval. One end of the specimen was completely fixed using the vise (fixed area: 10 mm × 10 mm), and the other end was placed on the edge of the vise. Here, the curvature radius of the specimen was approximately 40 mm if the curvature was constant. The curvature was determined so that the

京都大学
KYOTO UNIVERSITY

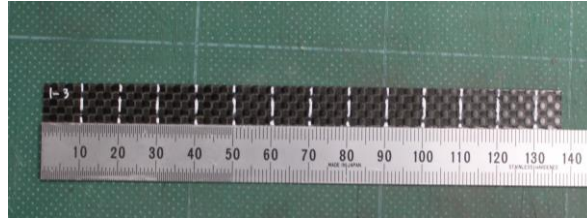M. Nishikawa, K. Nagata, Y. Naito, M. Hojo and N. Matsuda

Figure 2: Photograph of a specimen.

yielding of the matrix was avoided; the maximum strain of the specimen surface was about 0.25 %.

After releasing the constraint, the three-dimensional motion of the specimen was captured from two different directions on the specimen sides using stereo-photography. The used high-speed cameras were HAS-L1 (Ditect, lens: AI Nikkor 50mm f/1.4S (Nikon)). The photographing conditions were as follows; the shutter speed was 1/400 s, the frame rate was 300 fps, the image resolution of the cameras was 800×600, and the two cameras were synchronized. The obtained movies were processed using an image analysis software (DIPP-MOTION V/3D, Ditect); the images were obtained with 10 ms intervals, and the locations of the representative reference points in the images were identified in the software, and the three-dimensional coordinates of these points were obtained. The number of experiments was 2.

4 RESULTS AND DISCUSSION

First we explain the results of dynamic deployment tests. Here the initial time was defined as the time when the displacement direction of the reference points C and D changed.

Figure 3 shows the images of the specimen during the tests, obtained by the high-speed camera. As the stored elastic energy released, the tip of the specimen preferentially moved and the specimen returned to the original shape. Within about 30 mm from the fixed end, the local curvature of the specimen increased above initial curvature (0.025 /mm), and the bending deformation became large near the fixed end. This was caused by the tensile deformation in the length direction as the released tip of the specimen moved. After releasing the constraint, the specimen moved to the original shape, and then it was subjected to over-deformation (deflected toward the opposite direction). After that, the specimen started to oscillate and the deflection motion of the specimen successively occurred. The maximum amplitude of the oscillation was the maximum deflection during the first over-deformation.

The values of the deflection of the representative reference points A to D were defined as δ_A to δ_D, as illustrated in Fig. 4(a). Figure 4(b) presents the time history of the deflection δ_A to δ_D in the dynamic deployment tests. The missing lines in Fig. 4(b) were caused because the software fails to recognize the reference points due to the unclear marks in the images during the image processing.
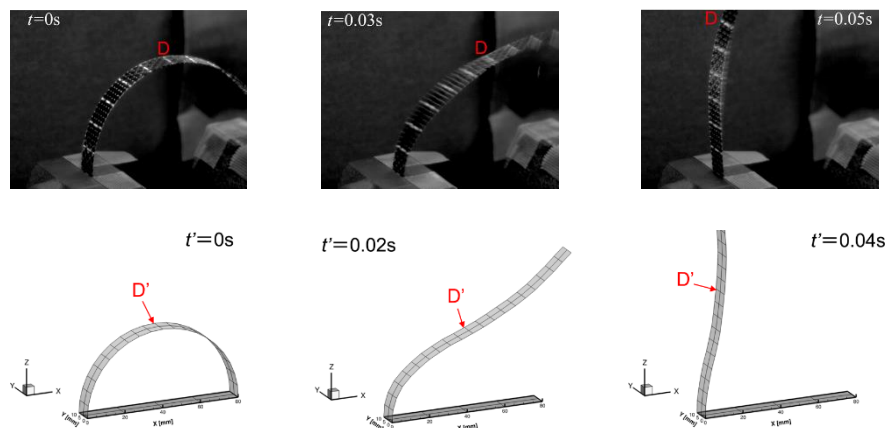

Figure 3: Comparison of deployment dynamics between experiment and simulation.

Specimen No.	Bending stiffness E_bI [N·m^2]	Bending modulus E_b [GPa]
1	174	19
2	153	18

Table 1: Estimated results of bending modulus of the specimen.

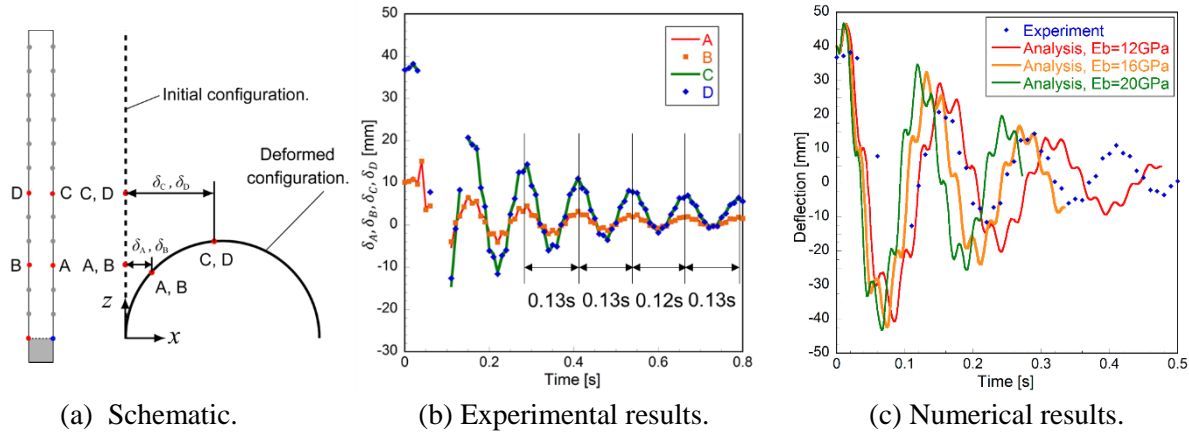(a) Schematic. (b) Experimental results. (c) Numerical results.

Figure 4: Details of the deformation of thin composite layer during the deployment.

From Fig. 4(b), we could find that the period of the oscillation cycles were almost constant. Although the deflection of a thin composite layer generally involves tension, bending and shear modes, the oscillation period became independent of the deflection amount in the experiment, from the comparison among four reference points A to D. Therefore, it was implied that the succeeding oscillation after the over-deformation at the first cycle was almost determined by the bending deformation of the specimen.

From the experimental fact that the oscillation period was almost constant, the bending modulus of the specimen could be evaluated. Here we assume that the oscillation observed in the experiment can be approximated by the bending oscillation of a cantilevered beam. Then the first natural angular frequency ω is related to the bending stiffness E_bI by the following equation [14].

$$\omega = 0.356 \frac{\pi^2}{l^2}\sqrt{\frac{E_bI}{\rho A}} \tag{3}$$

where A is the cross-sectional area of the specimen and l is the distance from the fixed end of the specimen. The estimated bending stiffness E_bI and bending modulus E_b using Eq. (3) were listed in Table 1. We conducted the experiments twice, and the estimated results were almost the same.

Figure 4(c) presents the numerical results of deployment motion at the reference point D ($l = 62.8$ mm, center of the specimen), in comparison with the experimental results, when the bending modulus was varied as 12, 16, and 20 GPa. Figure 5 shows the time history of the deformed configuration of the models. When the damping coefficient $\alpha = 0.01$ was used in the simulation, the decay of the oscillation in the numerical results were comparable to the experimental results, as found in Fig. 4(c). The bending modulus of the specimen had a significant influence on the deployment motion after releasing the constraint. Using the appropriate bending modulus for modeling the composites ($E_b = 16$ GPa), the simulated dynamics were almost similar to the experimental results, as compared in Fig. 4(c).

Figure 3 also presents the results of the detailed deformation during the deployment. The simulated results showed that the oscillation frequency became constant after the first few cycles as shown in Fig. 4(c). The different frequency of the first cycle was caused by the tension-bending coupled deformation after releasing the constraint. The converged oscillation frequency after the first few cycles was almost determined by the bending modulus of the composite layer, because the evaluated modulus based on the oscillation frequency (19 GPa) was close to the abovementioned value. In addition, the numerical results could appropriately reproduce the deployment dynamics including the tension-bending coupled deformation during the first deployment cycle and the subsequent bending oscillation, observed in the

(a) t =0s.　　　　　　(b) t =0.02s.　　　　　　(c) t =0.04s.

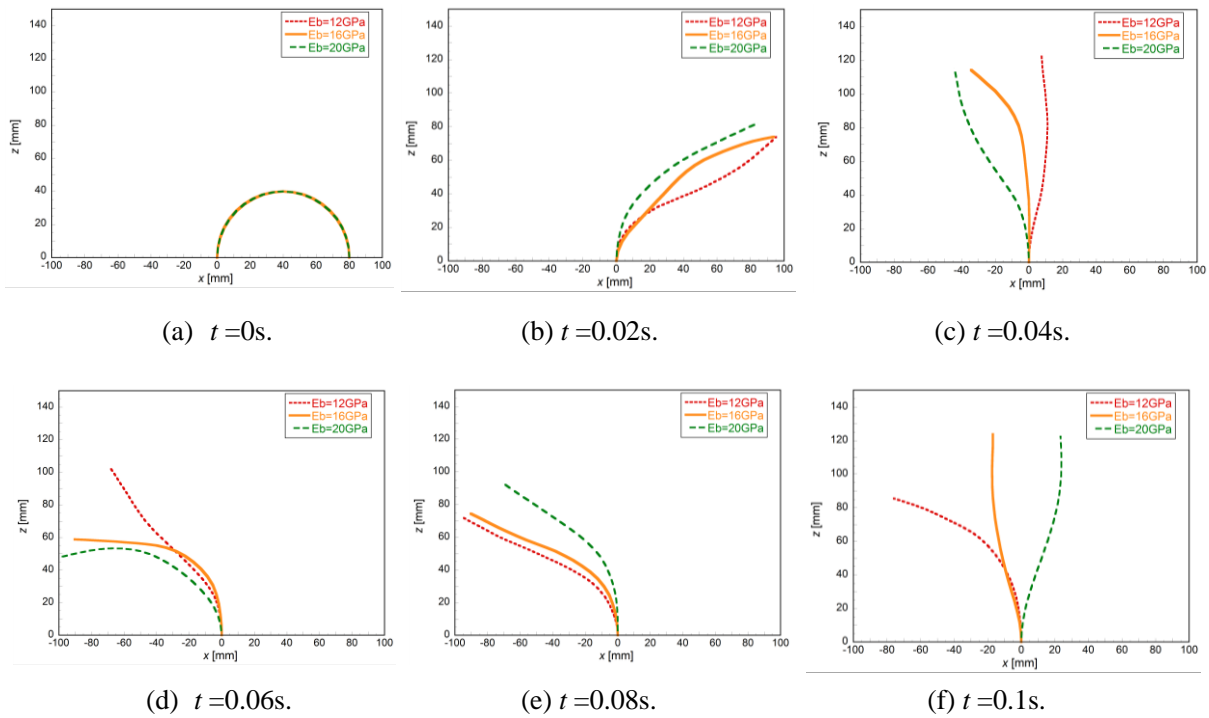(d) t =0.06s.　　　　　　(e) t =0.08s.　　　　　　(f) t =0.1s.

Figure 5: Time history of the deformed configuration in the simulation.

experiment.

In contrast, when the tensile modulus was varied as 16 GPa, 32.8 GPa, and 50 GPa, the simulated results hardly changed in our additional simulations. These results implied that the bending deformation was dominant in the present dynamic deployment tests, and that the bending modulus was appropriately determined using the natural angular frequency of the bending oscillation of the specimen in the experiment.

4   CONCLUSIONS

The present study attempted to reproduce the deployment tests of a thin composite layer made of CFRP plain-woven textile composite, using a newly developed dynamic deployment simulation. The simulation employed a three-layer model in the shell-element based dynamic explicit analysis, and the difference between tension and bending properties of a thin composite layer was appropriately modeled. The simulated results were comparable to the experimental results when the bending modulus was appropriately selected from the experimental bending oscillation frequency. Thus the proposed simulation will become an effective tool to reproduce the deployment dynamics of a thin composite layer.

In the present study, we did not use the characteristics of SMPCs for the deployment process. If we use SMPCs as the materials of the thin composite layer, the bending modulus during the deployment decreases by the softening due to the thermal activation. Moreover, the required time for thermally-activated deployment was longer (the order of 100 s), as revealed by our previous experiment [9]. Therefore, we should note that the bending oscillation may not be a key factor for the deployment dynamics of the SMPCs. The deployment sequence and the resulting shape change are a matter to be discussed in our future study.

REFERENCES

[1] T.W. Murphey and S. Pellegrino, A novel actuated composite tape-spring for deployable structures, Proceedings of the 45th AIAA/ASME/ASCE/AHS/ASC Structures, Structural Dynamics & Materials Conference, Reston, Virigina. 2004.

[2] M.R. Schultz, M. J. Hulse, P. N. Keller and D. Turse, Neutrally stable behavior in fiber-reinforced composite tape springs, *Composites A*, **39**, 2008, pp. 1012-1017.

[3] H.M.Y.C. Mallikarachchi and S. Pellegrino, Quasi-static folding and deployment of ultrathin composite tape-spring hinges, *Journal of Spacecraft and Rockets*, **48**, 2011, pp. 187-198.

[4] K. Gall, M. Mikulas, N. A. Munshi, F. Beavers and M. Tupper, Carbon fiber reinforced shape memory polymer composites, *Journal of Intelligent Material Systems and Structures*, **11**, 2000, pp. 877-886.

[5] J. Leng, X. Lan, Y. Liu and S. Du, Shape-memory polymers and their composites: stimulus methods and applications, *Progress in Materials Science*, **56**, 2011, pp. 1077-1135.

[6] J.H. Roh, H.J. Kim and J.S. Bae, Shape memory polymer composites with woven fabric reinforcement for self-deployable booms, *Journal of Intelligent Material Systems and Structures*, **25**, 2014, pp. 2256-2266.

[7] S. Chen, Y. Chen, Z. Zhang, Y. Liu and J. Leng, Experiment and analysis of morphing skin embedded with shape memory polymer composite tube, *Journal of Intelligent Material Systems and Structures*, **25**, 2014, pp. 2052-2059.

[8] J. Ishizawa, K. Imagawa, J. Yoshikawa, S. Hayashi and N. Miwa, Research on applicability of shape memory polymers (SMPs) to inflatable and deployable space structures, In: Proceedings of SAMPE Japan 2001, 2001.

[9] Y. Naito, M. Nishikawa and M. Hojo. Effect of reinforcing layer on shape fixity and time-dependent deployment in shape-memory polymer textile composites, *Composites A*, **76**, 2015, pp. 316-325.

[10] T. Sato, H. Sakamoto, K. Shintaku, G. Ono, S. Matsunaga, O. Mori, Y. Shirasawa, N. Okuizumi and M. Okuma, Research on non-synchronous deployment of spinning solar sail membrane considering crease stiffness, *Aerospace Technology Japan*, **13**, 2014, pp. 71-75 (in Japanese).

[11] M.A. Neto, J.A.C. Ambrosio and R.P. Leal, Composite materials in flexible multibody systems, *Computer Methods in Applied Mechanics and Engineering*, **195**, 2006, pp. 6860-6873.

[12] T.J. Keli and J.A. Banik, Stowage and deployment strength of a rollable composite shell reflector, 52nd AIAA/ASME/ASCE/AHS/ASC Structures, Structural Dynamics and Materials Conference 19th 4-7 April 2011, Denver, Colorado, AIAA 2011-2103.

[13] T. Hisada and H. Noguchi, Fundamentals and applications of nonlinear finite element method, Maruzen, Tokyo, 1995, pp. 223-225 (in Japanese).

[14] T. Iwatubo and T. Matsuhisa, Fundamentals of vibration engineering, Morikita, 2008, (in Japanese).